HHS Public Access

Author manuscript

Biochemistry. Author manuscript; available in PMC 2024 January 01.

Published in final edited form as:

Biochemistry. 2023 June 20; 62(12): 1864–1877. doi:10.1021/acs.biochem.2c00628.

The Y46D Mutation Destabilizes Dense Packing of the Second Greek Key Pair of Human γC-Crystallin Causing Congenital Nuclear Cataracts

Venkata Pulla Rao Vendra,
Ophthalmic Molecular Genetics Section, Ophthalmic Genetics and Visual Function Branch, National Eye Institute, National Institutes of Health, Bethesda, Maryland 20852, United States

Christian Ostrowski,
Ophthalmic Molecular Genetics Section, Ophthalmic Genetics and Visual Function Branch, National Eye Institute, National Institutes of Health, Bethesda, Maryland 20852, United States

Rebecca Clark,
Ophthalmic Molecular Genetics Section, Ophthalmic Genetics and Visual Function Branch, National Eye Institute, National Institutes of Health, Bethesda, Maryland 20852, United States

Marzena Dyba,
Biophysics Resource in the Center for Structural Biology, National Cancer Institute, National Institutes of Health, Frederick, Maryland 21702-4091, United States

Sergey G. Tarasov,
Biophysics Resource in the Center for Structural Biology, National Cancer Institute, National Institutes of Health, Frederick, Maryland 21702-4091, United States

J. Fielding Hejtmancik
Ophthalmic Molecular Genetics Section, Ophthalmic Genetics and Visual Function Branch, National Eye Institute, National Institutes of Health, Bethesda, Maryland 20852, United States

Abstract

The γ-crystallins are highly expressed structural lens proteins comprising four Greek key motifs arranged in two domains. Their globular structure and short-range spatial ordering are essential for lens transparency. Aromatic residues play a vital role in stabilizing Greek key folds by

Corresponding Author: **J. Fielding Hejtmancik,** – *Ophthalmic Molecular Genetics Section, Ophthalmic Genetics and Visual Function Branch, National Eye Institute, National Institutes of Health, Bethesda, Maryland 20852, United States*; Phone: 301-496-8300; hejtmancikj@nei.nih.gov.

Author Contributions

The manuscript was written through contributions of all authors. All authors have given approval to the final version of the manuscript.

The authors declare no competing financial interest.

ASSOCIATED CONTENT

Supporting Information

The Supporting Information is available free of charge at https://pubs.acs.org/doi/10.1021/acs.biochem.2c00628.

Figure S1: comparison of wild-type and Y46D mutant γC-crystallins under thermal and chemical stress; Tables S1–S7: masses from LC/MS analyses of wild-type human γC-crystallin + αA-crystallin size exclusion chromatography fractions (PDF)

Accession Codes

CRYAA mRNA: NM_000394; CRYAA protein: NP_001350695; CRYGC mRNA: NM_020989; CRYGC protein: NP_066269.

forming Greek key or non-Greek key pairs or tyrosine corners. We investigated the effects of the cataractogenic Y46D mutation in the second Greek key pair (Y46-Y51) of human γC-crystallin on its stability and aggregation. Wild-type and Y46D mutant human γC-crystallin were overexpressed in *E. coli* BL-21(DE3) PLysS cells, purified using ion-exchange and size-exclusion chromatography, and analyzed by fluorescence spectroscopy and circular dichroism spectroscopy. The Y46D mutation does not affect the γC-crystallin backbone conformation under benign conditions but alters the tryptophan microenvironment, exposing hydrophobic residues to the surface. The Y46D mutant undergoes a three-state transition under thermal stress with midpoints of 54.6 and 67.7 °C while the wild type shows a two-state transition with a midpoint of 77.6 °C. The Y46D mutant also shows a three-state transition under GuHCl stress with C_m values of 0.9 and 2.1 M while the wild type shows a two-state transition with a C_m of 2.4 M GuHCl. Mutant but not wild-type γC-crystallin forms light scattering particles upon heating at 65 °C. Overall, the Y46D CRYGS mutation leaves the protein fold intact under benign conditions but destabilizes the molecule by altering the tryptophan microenvironment and exposing hydrophobic residues to its surface, thus increasing its susceptibility to thermal and chemical stress with resultant self-aggregation, light scattering, and cataract.

Graphical Abstract

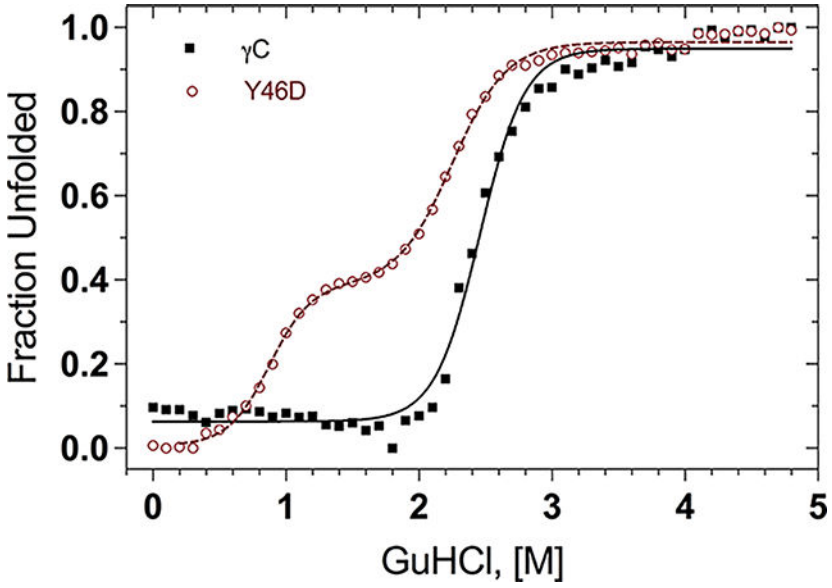

INTRODUCTION

The basic function of the eye lens is to transmit and focus light onto the retina. This requires that the fiber cells in the central lens be well-ordered and without organelles and that they should contain high concentrations of stable and tightly packed soluble proteins so that their refractive index remains constant over distances approximating the wavelength of the transmitted light.[1] Crystallins are highly soluble structural proteins that constitute over 90% of the total lens mass. They can be classified into three types, α, β, and γ,[2] with the β- and γ-crystallins forming a large gene family.[3] Their compact globular structure and short-range spatial ordering allow them to be present in the high concentrations that

provide the necessary refractive index to transmit and focus light on the retina.[4] Because the fiber cells of the lens nucleus lack organelles and cannot carry out protein synthesis, the crystallins that populate the central lens must maintain their structure for the life of the organism.[5] Thus, any variation that affects their stability and compact packing results in poor refraction and light scattering, causing clinical cataract. Currently, at least 60 loci, for 40 of which the causative genes and mutations have been identified, have been associated with congenital cataracts, and the causative mutations in approximately 33% of independent families occur in crystallin genes.[6]

Human γC-crystallin is a 174 amino acid protein comprising two homologous domains, each domain consisting of two extremely stable Greek key motifs.[7–9] These consist of four β-sheets arranged antiparallel to each other, forming a (3,1) C type of Greek key motif with (−1, −1, +3) topology in which the third strand of the adjacent Greek key motif joins the first Greek key motif.[10] The structural integrity of Greek key motifs in the βγ-crystallins is an essential element in their stability and compact packing.[11] The aromatic amino acids phenylalanine, tyrosine, and tryptophan play an important role in stabilizing folding of Greek key motifs. The human γC-crystallin protein includes 4 phenylalanine, 14 tyrosine, and 4 tryptophan residues. Of these 22 aromatic amino acids, 14 are involved either in pairing with an aromatic partner 5 or 13 residues distant (forming a “Pair”) or participating in “Tyrosine corners”. Tyrosine corners are classic features of Greek key motifs in which the hydroxyl groups of two tyrosines form hydrogen bonds with a backbone carboxyl group of tryptophan, holding the two adjacent β-strands forming the Greek key motif together. The γ-crystallins have two Δ4 type tyrosine corners, one in each domain.[7] They also have three aromatic pairs separated by 5 amino acids present in Greek keys and hence are referred to as Greek Key pairs (Y7-F12, Y46-Y51, and Y134-Y139) and another pair, Y17-Y29, separated by 13 amino acids is a non-Greek key pair. Two tyrosine corners (Y56-Y63-W69 in the N-terminal domain and Y144-Y151-W157 in the C-terminal domain) are present in both γC- and γD-crystallins.[12] The aromatic rings in the aromatic pairs are arranged parallel[13] or perpendicular[14] to each other with an optimal distance of 4.5–7 Å, with each contributing about 0.6–1.3 kcal mol^{-1} to the stability of the protein.[14,13]

Mutations that replace those phenylalanines or tyrosines participating in aromatic pairs are predicted to destabilize the γ-crystallins significantly. A c.136 T>G (p.Y46D) mutation in CRYGC, which disrupts the Y46-Y51 tyrosine pair in the second Greek key motif of human γC-crystallin, has been associated with autosomal dominant congenital nuclear cataracts.[15] Recent work by Fu et al.[16,17] showed that the Y46D and L45P mutations decrease the UV light, oxidative, pH, chemical, and thermal stability of γC-crystallin. Here, the effect of the Y46D mutation on the structure and stability of γC-crystallin was further investigated and extended to include the aggregate sizes and effects of α-crystallin binding and reducing agents on this process and to calculate the thermodynamic stabilities of the wild-type and mutant proteins in order to elucidate the possible molecular mechanisms responsible for the cataracts in this family.

MATERIALS AND METHODS

Cloning and Site-Directed Mutagenesis.

Human γC-crystallin cDNA was cloned into the *Nde*I/*Hind*III s*ites* of the pET-21a (+) vector as described earlier.[18] To generate the Y46D mutant clone, the wild-type clone was amplified with the following primers F-5′-CTGGATGCTCGATGAGCGTCCCAACTACCAAGG-3′, R-5′-GGGACGCTCATCGAGCATCCAGCAGCC-3′. Methylated wild-type DNA was eliminated by digesting with *Dpn*I, and the resultant plasmids were transformed into *E. coli* DH5α. Plasmids were isolated from the transformed *E. coli* colonies and bidirectionally sequenced to confirm the base pair changes and the absence of nonspecific mutations. Human αA-crystallin cDNA was cloned into the *Nde*I/*Xho*I s*ites* of pET-21a (+) (Novagen) using a reverse primer harboring a CACCACCACCACCACCAC (6X his tag) sequence just before the stop codon.

Protein Overexpression.

Proteins were overexpressed and purified as described earlier.[19,20] Briefly, BL21(DE3) pLysS cells were used to express the wild-type and mutant proteins. A single colony containing the clone was inoculated into 12 mL of LB broth containing 50 μg/mL ampicillin and 34 μg/mL chloramphenicol and grown for 12 h at 37 °C with 225 rpm shaking. 10 mL of this grown culture was transferred to 1 L of LB broth with the same concentration of antibiotics. The inoculated broths were grown till they reach an OD of 0.6–0.8. The cultures were adjusted to a final concentration of 0.5 mM IPTG and grown at 37 °C for an additional 4 h. Induced cells were pelleted by centrifugation at 6000*g* for 10 min at 4 °C and frozen at −80 °C until use.

γC-Crystallin (UniProtKB-P07315) Purification.

Pellets containing cells with overexpressed proteins were resuspended in 50 mM Tris-Cl pH 7.3, 100 mM NaCl, 1 mM ethylenediaminetetraacetic acid (EDTA), 1 mM dithiothreitol (DTT), 250 μM tris(2-carboxyethyl)phosphine (TCEP), and a protease inhibitor mix (Thermo Scientific Pierce Protease Inhibitor Mini Tablets, Roche Diagnostics, Indianapolis, catalog no. 11836153001). The cell suspensions were brought to a final lysozyme concentration of 0.3 mg/mL and final DNase concentration of 7.5 μg/mL. Cell suspensions were freeze thawed for 4 cycles, each cycle consisting of a 5 min incubation on dry ice and 5 min incubation in a 37 °C water bath. The freeze-thawed cell suspension was further sonicated in an Omni international Sonic Ruptor-400 sonicator at 20% amplitude for the mutant 10 cycles, each cycle comprising a 5 s pulse on and 55 s pulse off and for wild-type using 6 cycles, each cycle comprising a 10 s pulse on and 50 s pulse off with a sonic rupture at 4 °C. The cell lysate was centrifuged at 30,000*g* for 20 min at 4 °C, and the supernatant was loaded into an 8 mL 10,000 MWCO dialysis cassette (Pierce) and dialyzed against 2 L of buffer A (20 mM Tris-Cl, 1 mM EDTA, 1 mM DTT, 50 μM TCEP, pH 8.4) for 3 h.

Soluble protein extracts were purified at room temperature by ion-exchange followed by size-exclusion chromatography using an NGC chromatography system (BIO-RAD). The dialyzed supernatant was centrifuged at 30000*g* for 20 min at 4 °C, and samples were loaded

onto a 5 mL HiTrap Q FF (GE Healthcare; catalog no.17–5156-01) column equilibrated with buffer A at a flow rate of 1.0 mL/min. HiTrap Q FF is a strong anion exchange chromatography column. After washing with five column volumes of buffer A, buffer B (20 mM Tris-Cl, 1 mM EDTA, 1 mM DTT, 50 μM TCEP, pH 8.4, and 1 M NaCl) was applied as a linear gradient through the column and fractions were collected. Both the wild-type and Y46D mutant γC-crystallin eluted at approximately 250 mM NaCl.

Fractions containing the protein of interest as monitored by A280 and SDS-PAGE were pooled, concentrated to 1.2 mL at 10–15 mg/mL by loading onto Amicon Ultra-15 centrifugal filter units (Millipore; Catalog no. UFC901024 18–004590) and centrifuging at 3500 rpm for 40 min at 4 °C. WT and Y46D γC-crystallin mutant samples were loaded onto a 120 mL HiPrep 16/60 Sephacryl S-100 HR (GE Healthcare; catalog no. 17116501) column pre-calibrated with five standards: thyroglobulin, γ-globulin, ovalbumin, myoglobin, and vitamin B12 (Bio Rad gel filtration standard; catalog no. 1511901) and equilibrated with SEC buffer: 50 mM Tris-Cl, 0.15 M NaCl, 1 mM EDTA, 1 mM DTT, and 50 μM TCEP at a flow rate of 0.5 mL/min. The location of recombinant proteins in column fractions was monitored by absorbance at 280 nm and by SDS-PAGE on 12% polyacrylamide gels. Samples containing the protein of interest were pooled and concentrated to 5–10 mg/mL. The purity of the purified protein was assessed and confirmed by showing a single band on SDS PAGE and comparing the mass by ESI-LC/MS. Four independent preparations for each batch of γC wild-type and Y46D mutant proteins gave an average mass of 20745.55 ± 0.5 and 20697.11 ± 0.5 Da, respectively, using ESI-LC/MS, in agreement with the predicted monomer masses.

αA-Crystallin (UniProtKB-P02489) Purification.

αA-Crystallin with a His tag attached to the carboxy terminal end was also purified using a modification of the above-described method. The lysis buffer used in purifying αA crystallin was 50 mM KH_2PO_4/K_2HPO_4 pH 8.0, 300 mM KCl, 1 mM EDTA (buffer C) with a protease inhibitor mix (Roche Diagnostics; catalog no. 11836153001). Sonication was done as described above for the wild-type protein (6 cycles, each cycle comprising a 10 s pulse on/50 s pulse off) and the centrifuged cell lysate was loaded onto a HisTrap HP (GE Healthcare; catalog no. 17524801) column equilibrated with buffer C at a flow rate of 1.0 mL/min. Five column volumes of buffer C was passed through the column to wash off the unbound proteins completely, then a linear gradient of buffer D (50 mM KH_2PO_4/K_2HPO_4 pH 8.0, 300 mM KCl, 1 mM EDTA, and 0.5 M imidazole) was applied, and fractions were collected. Because the His tag had no effect on the αA-crystallin function when compared with the untagged protein, it was not removed before use in assays. αA samples were further purified by size exclusion chromatography as above using a HiPrep 16/60 Sephacryl S-300 HR (GE Healthcare; catalog no.17116701). Four independent preparations for each batch of αA-crystallin gave an average mass of 20731.06 ± 1 using ESI-LC/MS, in agreement with the predicted monomer mass.

ESI-LC/MS.

Mass spectrometry data of 0.1 mg/mL proteins samples (in 50 mM Tris-Cl (pH 7.3), 150 mM NaCl, and 50 μM TCEP buffer) were acquired on an Agilent 6130 Quadrupole LC/MS

System (Agilent Technologies, Inc., Santa Clara, CA) equipped with an electrospray source, operated in positive-ion mode. Separation was performed on a 300SB-C3 Poroshell column (2.1 mm × 75 mm; particle size 5 μm). The analytes were eluted at a flow rate of 1 mL/min with a 5 to 100% organic gradient over 5 min and holding an organic gradient for 1 min. Mobile phase A contained 5% acetic acid in water, and mobile phase B was acetonitrile.

Data acquisition as well as data analysis and deconvolution of mass spectra was performed using Open lab Chem Station Edition software (version C.01.05).

Circular Dichroism Measurements.

For determining the secondary structure, 0.25 mg/mL protein samples in 10 mM NaH_2PO_4/Na_2HPO_4 (pH 7.3) solution were scanned between 260 and 185 nm at 25 °C in a 1 mm pathlength cuvette using a 420SF circular dichroism instrument (Aviv Biomedical, Lakewood, NJ). A bandwidth of 1 nm and averaging time of 5 s at each point were maintained. The spectra were corrected for the background buffer signal. For near-UV CD spectra, 0.8 mg/mL samples in 50 mM NaH_2PO_4/Na_2HPO_4 (pH 7.3), 150 mM NaCl, and 50 μM TCEP were recorded between 350 and 250 nm at 25 °C in a 1 cm pathlength cuvette using a circular dichroism instrument J-1500 (JASCO, Easton, MD). The spectra were corrected for the background buffer signal. A bandwidth of 1 nm, scanning speed of 50 nm/min for near-UV CD, and DIT of 4 s at each point were maintained. At least five independent runs were measured and averaged, and spectra for the corresponding buffer for each protein were subtracted. For determining the secondary structure of wild-type and mutant proteins under GuHCl induced stress, 0.15 mg/mL protein samples in 10 mM NaH_2PO_4/Na_2HPO_4 (pH 7.3) solution were incubated with varying concentrations of GuHCl (0–5 M, prepared by serial dilution of a 5 M stock solution) for 12–14 h at room temperature, and circular dichroism was measured between 260 and 185 nm at 25 °C in a 1 mm pathlength cuvette as described above. Three independent runs were measured and averaged, and blank spectra of the corresponding buffer were subtracted for each protein.

Thermal denaturation experiments were performed by heating the proteins from 25–95 °C with a ramping rate of 1 °C/min and collecting the 218 nm CD signal using a 420SF CD instrument. The protein concentration was 0.5 mg/mL in 50 mM NaH_2PO_4/Na_2HPO_4 (pH 7.3), 150 mM NaCl, and 50 μM and 0.25 mM TCEP buffer. Samples were equilibrated for 60 s at each 1 °C step. The temperature dead band was 0.2 °C, and the averaging time was 5 s. Thermal denaturation curves were analyzed using GraphPad Prism 7 software according to the method of Pace et al.[21,22] The enthalpy change, ΔH, was calculated using the van't Hoff equation: $d(\ln K)/d(1/T) = -\Delta H/R$. ΔG values were calculated using the equation $\Delta G = -RT \ln K$.

To check protein stability at elevated temperatures, 0.15 mg/mL samples of protein in 50 mM NaH_2PO_4/Na_2HPO_4 buffer were heated to 54.5 and 67.5 °C and ellipticity at 218 nm was monitored as a function of time. The parameters maintained in monitoring the thermal denaturation experiments were used for these experiments as well.

Fluorescence Spectroscopic Measurements.

For measuring tertiary structure by tryptophan fluorescence emission, the 0.05 mg/mL solution of protein in 56.25 mM NaH_2PO_4/Na_2HPO_4 (pH 7.3), 150 mM NaCl, 1 mM EDTA, 5 mM DTT, and 50 μM TCEP buffer was excited with 295 nm wavelength light and the emission was collected between 300 and 400 nm using a FluoroMax-4C (Horiba Instruments, Piscataway, NJ) with excitation emission slits of 2.5 nm and integration times of 1 s. Spectra were corrected for the background buffer signal. For thermal denaturation studies the 355/330 nm ratio was used to plot the curves as described above. Three independent runs were measured, and values for the corresponding buffer were subtracted as a blank for each protein. The 355/330 nm fluorescence ratio was measured as a function of temperature with λ_{exc} of 285 nm. Protein samples of 0.5 mg/mL in 50 mM NaH_2PO_4/ Na_2HPO_4 (pH 7.3), 150 mM NaCl, and 50 μM TCEP buffer were heated from 25–95 °C with 1 °C/min ramping. For determining the tertiary structure of wild-type and Y46D mutant proteins under GuHCl induced stress, 0.1 mg/mL protein samples in 50 mM NaH_2PO_4/ Na_2HPO_4 (pH 7.3), 150 mM NaCl, 1 mM EDTA, 5 mM DTT, and 50 μM TCEP buffer were incubated with varying concentrations of GuHCl (0–5 M) for 12–14 h at room temperature and tryptophan emission was collected between 300 and 400 nm at 25 °C by exciting the samples at 295 nm with excitation/emission slits of 10 nm and integration time of 1 s. The GuHCl did not interfere with fluorescence measurements, and any background due to GuHCl was subtracted from all measurements. For measuring the effects of α-crystallin on γC-crystallin denaturation, 2.5 μM protein samples in 50 mM Tris-Cl (pH 7.3) and150 mM NaCl buffer were heated at 65 °C for 1100 s and light scattering was monitored at 600 nm. For measuring the effects of reducing agents on Y46D γC-crystallin denaturation, the samples were heated at 65 °C in the absence and presence of DTT or TCEP over the times shown in the figures.

Surface hydrophobicity and aggregation propensities were assessed using bis-ANS[23] and Nile Red.[24] Samples with 0.33 mg/mL protein in 66.7 mM NaH_2PO_4/ Na_2HPO_4 (pH 7.3), 150 mM NaCl, 1 mM EDTA, 5 mM DTT, and 50 μM TCEP buffer were incubated with a final concentration of (0.58–74.31 μM) bis-ANS in the dark at room temperature for 30 min. Spectra with bis-ANS were recorded between 400 and 600 nm by exciting the samples at 390 nm. For Nile Red experiments, 0.1 mg/mL protein samples in 52.5 mM NaH_2PO_4/ Na_2HPO_4 (pH 7.3), 150 mM NaCl, 1 mM EDTA, 5 mM DTT, and 50 μM TCEP buffer were incubated with (0.08–19.63 μM) dye in the dark for 30 min. Nile Red samples were excited at 540 nm, and emissions were collected between 570 and 700 nm. Fluorescence intensities at 490 nm (bis-ANS) and 650 nm (Nile Red) were plotted against the dye concentration.

Formation of amyloid fibrils under physiological conditions (not acidified) was checked using Thioflavin-T.[25] 0.1 mg/mL protein samples in 52.5 mM NaH_2PO_4/Na_2HPO_4, (pH 7.3), 150 mM NaCl, 5 mM DTT, 1 mM EDTA, and 50 μM TCEP buffer were incubated in the dark for 30 min, with a final concentration of 5–125 μM thioflavin-T dye, and spectra were recorded between 470 and 570 nm by exciting the samples at 444 nm.

For GuHCl unfolding experiments, samples with a final concentration of 0.15 mg/mL protein in 55 mM NaH_2PO_4/Na_2HPO_4 (pH 7.3), 165 mM NaCl, 5 mM DTT, 1 mM EDTA, and 55 μM TCEP buffer were equilibrated at room temperature for 12–14 h with stepwise

increments of 0.1 M GuHCl and spectra were recorded at each step after equilibration. For refolding experiments, 1.0 mg of wild-type and mutant proteins were incubated at the final concentration of 5 M GuHCl, 64 mM NaH_2PO_4/Na_2HPO_4 (pH 7.3), 191 mM NaCl, 5 mM DTT, 1 mM EDTA, and 64 μM TCEP buffer at room temperature for 7 h, then diluted into a series of tubes containing refolding buffer 56 mM NaH_2PO_4/Na_2HPO_4 (pH 7.3), 170 mM NaCl, 5 mM DTT, 1 mM EDTA, and 56 μM TCEP buffer with varying final concentrations of 0.1–4.8 M GuHCl (at 0.1 M GuHCl decrements), and allowed to equilibrate at room temperature for 18 h. The spectral conditions were the same as for unfolding experiments. GuHCl unfolding and refolding curves were analyzed by plotting the concentration of GuHCl for each sample versus the ratio of fluorescence intensities at 355 nm (maximum for the unfolded protein) and 330 nm (maximum for the native protein), as described by Kong and King.[12] The ratio of fluorescence intensities at these wavelengths was chosen for the analysis to simultaneously monitor changes in the native and unfolded maxima. Equilibria unfolding/refolding data were analyzed using GraphPad Prism 7 software, and $\Delta G°$ and m values were calculated using the method of Pace.[22]

For 65 °C thermal aggregation studies, proteins at a final concentration of 2.5 μM protein in 50 mM Tris-Cl (pH 7.3) and 150 mM NaCl buffer were heated to 65 °C and static light scattering was measured at 600 nm using a spectrofluorometer for 1100 s.

All fluorescence experiments were carried out at 25 °C and 2.5 nm excitation/emission slits and 1 s integration time at each point was maintained. Excitation and emission slits of 10 nm were used in GuHCl unfolding and refolding experiments.

Differential Scanning Fluorimetry Measurements.

Thermal denaturation was also probed by tryptophan emission using a differential scanning fluorimeter Prometheus NT.48 (NanoTemper Technologies GmbH, Munich, Germany), and the same protein concentrations and buffer strengths were maintained as for CD thermal unfolding experiments. Samples were heated from 25–95 °C and excited at 285 nm, and the 355/330 nm emission ratio was collected as a function of temperature.

DLS Measurements.

Wild-type and mutant protein particle sizes and distributions were assessed by dynamic light scattering using a DynaPro NanoStar dynamic light scattering instrument (Wyatt Technology, Santa Barbara, CA). Protein solutions of 37.5 μM in 50 mM Tris-Cl (pH 7.3) and 150 mM NaCl buffer were illuminated by 658 nm laser, and light scattered at a 90° angle was measured from 32–56.5 °C in 3.5 °C increments. A minimum of 20 acquisitions at each temperature step was recorded. Each protein solution was analyzed twice, and the average of all acquisitions is presented. A 1 °C/min ramping rate and equilibration time of 2 min at each temperature were maintained before collecting acquisitions. To obtain the hydrodynamic radii the intensity autocorrelation functions were fitted by a regularization algorithm using Dynamics software version 7.10 (Wyatt Technology, Santa Barbara, CA).

Analytical Size Exclusion Chromatography.

Proteins at a final concentration of 37.5 μM were incubated at room temperature, 45, 50, and 55 °C for 60 min in the presence an 8:1 molar ratio of αA-crystallin in 50 mM Tris-Cl (pH 7.3) and 150 mM NaCl buffer before being injected into a 24 mL ENrich SEC650 (Bio-Rad # 780–1650) column equilibrated with 2 column volumes of 50 mM Tris-Cl (pH 7.3) and 150 mM NaCl. A flow rate of 0.5 mL/min was maintained, and the sample volume injected was not more than 1% of the column volume (240 μL). Incubation of the Y46D mutant γC-crystallin at 55 °C resulted in visible precipitates, and it was not analyzed.

αA-Crystallin and γC-Crystallin Association.

αA-Crystallin association with the mutant and wild-type protein was also analyzed using analytical size exclusion chromatography. Mutant and wild-type protein at a final concentration of 37.5 μM were combined with αA-crystallin at a final concentration of 300 μM in 50 mM Tris-Cl (pH 7.3) and 150 mM NaCl solution. A molar excess of αA-crystallin was used to maximize binding to the γC-crystallin proteins.[26] The solutions were incubated at room temperature, 45, 50, or 55 °C for 1 h. The Y46D mutant protein aggregated upon heating at 55 °C and was not further analyzed. The samples were then injected into a 24 mL ENrich SEC650 (Bio-Rad # 780–1650) column equilibrated with 2 column volumes of 50 mM Tris-Cl (pH 7.3) and 150 mM NaCl. A flow rate of 0.5 mL/min was maintained, and the sample volume injected was not more than 1% of the column volume (240 μL). Eluted fractions were analyzed using ESI LC/MS.

RESULTS

The backbone conformations of wild type and Y46D mutant γC-crystallins were examined by measuring the molar ellipticity in the far-UV region (260–185 nm). The spectra are similar (Figure 1A), with a prominent negative band at 218 nm indicative of β-sheet conformation and a short arm around 206 nm, which is contributed by α-helical content. The overall backbone conformation is not altered and the differences in the molar ellipticities at 206 and 218 nm are very minor, consistent with the mutation not distorting the protein fold under benign conditions. To check the stability of wild-type and mutant proteins under GuHCl induced stress, both proteins were incubated with varying concentrations of GuHCl (0–5 M) for 12–14 h and far-UV CD spectra were recorded. The β-sheet conformation of the wild type was comparatively stable through 2 M GuHCl (Figure 1B), but the mutant started losing β-sheet conformation from 1 M GuHCl (Figure 1C) and beyond 2 M GuHCl, the mutant's backbone conformation was largely lost. We were unable to record CD spectra below 206 nm with GuHCl samples due to high HT voltages.

In addition, the tertiary structure was assessed by circular dichroism in the near-UV region and by monitoring tryptophan emission florescence by fluorescent spectroscopy. The near-UV CD spectra of wild-type and mutant show a similar pattern and peaks with varying molar ellipticity intensities (Figure 1D). However, the wild-type showed an ellipticity of −37.3 and −25.4 units, whereas mutant showed −10.4 and +10.8 units at 295 and 288 nm, respectively, consistent with altered microenvironments around tryptophan and tyrosine residues in the Y46D mutant γC-crystallin protein molecule. The tryptophan emission

spectra are more informative than the circular dichroism, as human γC-crystallin has four well-buried tryptophans at positions 43, 69, 131, and 157 (first methionine is counted) and all of them are excellent chromophores in emitting fluorescence. When the wild-type and mutant proteins were scanned between 300 and 400 nm by exciting the solution selectively at 295 nm, the tryptophan emission spectra differ according to their exposure to the aqueous environment on the surface. The wild type and mutant spectra show clear differences with the Y46D mutant showing approximately 1.2-fold higher fluorescence and a redshift of 1 nm from 329 to 330 nm compared to the wild type (Figure 1E). Thus, while the protein fold shows minimal distortion, the tryptophan microenvironment is altered to some degree. In order to assess the mutant's stability compared to the wild-type protein, the tertiary structure under GuHCl-induced stress was also recorded. The emission maxima of the wild-type are 330 nm at 0, 1, and 2 M GuHCl (Figure 1F), suggesting that in the wild-type protein, the tryptophan microenvironments are intact until 2 M GuHCl, whereas the mutant showed emission maxima of 330, 338, and 347 nm at 0, 1, and 2 M GuHCl, respectively (Figure 1G). This further indicates a tryptophan microenvironment in the mutant has begun to alter by 1 M GuHCl. Both proteins were unfolded essentially completely by 3 M GuHCl, showing higher tryptophan fluorescence compared to their native forms.

The surface hydrophobicity of the wild type and Y46D mutant γC-crystallins was probed with two different dyes: bis-ANS (4,4'-dianilino-1,1′-binaphthyl-5,5′-disulfonic acid)[23] and Nile Red (9-diethylamino-5-benzo phenoxazine).[24] The mutant shows significantly greater fluorescence compared to the wild type exposed to 0.58–74.31 μM bis-ANS (Figure 2A). The Y46D mutant fluorescence was similar to that of the wild type at concentrations of Nile Red up to 5 μM and then increased to approximately 1.4 times the wild type at a dye concentration of 19.63 μM dye (Figure 2B). Both these experiments confirm that the mutant surface is more hydrophobic compared to the wild type, although the difference with the bis-ANS is much more dramatic. The relative tendencies of the Y46D and wild-type γ-crystallin to form amyloid fibrils were checked by incubating the mutant and wild-type protein with Thioflavin-T, a well-known dye for characterizing amyloid fibril formation.[25] The incubation was carried out under relatively physiological conditions (not at extreme temperature and pH values), and fluorescence was monitored at 485 nm. The wild-type and Y46D mutant γC-crystallins do not show a significant difference, although the mutant shows a slightly lower fluorescence at all concentrations (Figure 2C). Thus, neither the wild type nor the Y46D mutant γC-crystallin tend to form amyloid aggregates readily under physiological conditions and the Y46D mutation does not tend to increase amyloid formation under these conditions.

The stability of the Y46D mutant versus the wild-type γC-crystallin was assessed by heating the proteins slowly from 25 to 95 °C while monitoring the ellipticity at 218 nm, the characteristic wavelength of antiparallel β-sheet and the peak wavelength monitored in the initial secondary structure assessment. The wild-type protein followed a sharp two-state transition, whereas the transition curve of the Y46D mutant was more gradual, showing a shoulder between 50 and 60 °C, indicating a three-state transition with an intermediate (Figure 3A–C). A similar but more pronounced trend was observed when the thermal stability was monitored with tryptophan emission fluorescence (Figure 3D–F), although by the end of the temperature curve, both proteins had become turbid and turned opaque.

Plots of ΔG values calculated from the above thermal denaturation curves are shown in Figure 3B,E. All three lines in both plots are distinctly distanced and directed downward with varying slopes. The plot based on CD data of the wild-type γC-crystallin shows a slope of 0.478 kcal mol^{-1} $deg.^{-1}$, while the first and second transitions slopes of the Y46D mutant show slopes of 0.202 and 0.311 kcal mol^{-1} deg^{-1}. The transition midpoint for the wild-type γC-crystallin was 77.6 °C, whereas the first and second transition midpoints for Y46D mutant were 54.6 and 67.7 °C, respectively. From these plots, the mutant shows an equilibrium ΔH value of 66.2 kcal mol^{-1} for the first transition and 106.1 kcal mol^{-1} for the second transition, while the wild type shows a ΔH of 167.6 kcal mol^{-1}. The lower T_m values and the smaller ΔH values of the Y46D mutant are consistent with the first derivative curves derived from the thermal denaturation experiment, in which the Y46D mutant displays a clear three-state transition with two first derivate peaks, one in the range of 40–60 °C and the second one around 60–76 °C (Figure S1A), but the WT CD unfolding shows only a single first derivative peak at 60–76 °C. In thermal denaturation experiments monitored by the fluorescence ratio shown in Figure 3D, the Y46D mutant protein demonstrates a three-state curve with transitions a 52.9 and 68.0 °C, while the WT shows a two-state curve with a single transition at 77.4 °C. The ΔG values, T_m values, and slopes are consistent with those of the CD results overall but varied slightly (Table 1), perhaps because of different probing methods and equilibration times at each temperature in the two technologies. The van't Hoff plots also follow similar trends (Figure 3C,F). The relative thermal stability was also checked by heating the wild type and Y46D mutant at 54.5 °C (T_m of the first transition) and 67.5 °C (T_m of the second transition) while monitoring the CD signal at 218 nm. The mutant loses its structure completely by around 10 min when heated at 67.5 °C (Figure S1B) but does not show a major effect at 54.5 °C, even after 30 min of incubation. The wild type is also stable and does not show any structural changes after being heated at 67.5 °C for 30 min, further confirming the decreased stability of the mutant under thermal stress.

In addition to thermal stress, GuHCl-induced chemical stress was also used to assess the thermodynamic stabilities of the wild-type and Y46D mutant γC-crystallins. The fluorescence intensity ratio at 355/330 nm was used to monitor levels of the unfolded and native states. The wild-type protein shows a sharp two-state transition while the mutant shows a broader three-state transition with an intermediate form (Figure 4A), and the transition midpoint, apparent m values, and ΔG values calculated from the GuHCl unfolding curves are shown in Table 2. Unfolding of the N-terminal domain is seen between 0 and 2.0 M GuHCl with a concentration midpoint of 0.9 M in the mutant, consistent with the destabilization of the N-terminal domain seen with thermal denaturation, whereas unfolding of the wild-type N-terminal and C-terminal domains is not clearly distinct and shows a sharp transition around 2.4 M GuHCl. Unfolding of the mutant C-terminal domain is also affected by the Y46 to D mutation, with the concentration midpoint decreasing to 2.1 M GuHCl. ΔG values were calculated from the equation $\Delta G = -RT \ln K$, where R is the universal gas constant (1.987 cal/mol K), T is in Kelvin, and K is a factor that varies with GuHCl concentration. Plots of ΔG versus the GuHCl concentration (Figure 4B,D) follow the same trend as those seen in the thermal denaturation curves. The wild-type γC-crystallin shows an equilibrium ΔG value of 10.503 kcal mol^{-1} whereas the mutant shows ΔG values of 3.218 and 6.171 kcal mol^{-1} for N and C-terminal domains, respectively. Once more, the

lower transition midpoint GuHCl concentrations and the smaller ΔG values of the Y46D mutant are consistent with the first derivative curves derived from the GuHCl denaturation experiment, in which the Y46D mutant displays a clear three-state transition with two first derivate peaks, one in the range of 0.9 M GuHCl and the second one around 2.1 M GuHCl, while the wild type unfolding curve shows only a single first derivative peak at 2.4 M GuHCl (Figure S1C).

The GuHCl refolding curves and the corresponding ΔG plots are similar to the unfolding experiments except that they show some off-pathway aggregates at lower GuHCl concentrations (0–1.0 M GuHCl, Figure 4C,D), which is often observed with human γD-crystallin in refolding experiments.[27] In addition, the N-terminal transition was not as clear as that observed in the unfolding experiments, although the overall characteristics were quite similar, with the mutant showing two transitions, around 1.5 and 2.2 M, and the wild type exhibiting a single transition around 3.0 M (Figure 4C, Figure S1D). Because the interference of off-pathway aggregates made the first transition less clear, the Y46D mutant C_m, ΔG, and apparent m values were calculated only for the second transition for the renaturing curves. While the values were similar overall, there were some small differences between the unfolding and refolding parameters of both the wild-type and Y46D γC-crystallin mutant (Table 2).

Transparency under thermal stress was measured by static light scattering at 600 nm as a function of time at 65 °C. Wild-type γC-crystallin did not scatter visible light appreciably throughout the duration of the experiment, but light scattering by the Y46D mutant γC-crystallin started at around 150 s (Figure 4E), increasing linearly until around 500 s, indicating the tendency of the mutant to denature, aggregate, and form light scattering particles at elevated temperatures. Scattering was significantly inhibited by addition of a 1:1 molar ratio of αA-crystallin, indicating the ability of αA-crystallin to associate with the partially denatured mutant under thermal stress and prevent formation of large aggregates. After 1100 s, the wild-type γC-crystallin solution was clear and transparent but the mutant was opaque, showing visible aggregates. In contrast to αA-crystallin, reducing agents, including DTT and TCEP, do not prevent light scattering by the Y46D mutant γC-crystallin (Figure 4F).

The particle size of wild-type and Y46D mutant γC-crystallins with and without αA-crystallin under benign and thermal stress conditions was estimated by dynamic light scattering (Figure 5). Wild-type γC- and αA-crystallin maintained small radius equivalents throughout the temperature range, with γC-crystallin showing a narrow distribution at 1–2 nm and αA-crystallin showing a dispersed size distribution centering on 10 nm (Figure 5A,E). When αA-crystallin and wt γC-crystallin are heated together, the size distribution is simply the overlay of these two patterns for all temperatures through 56 °C (Figure 5B). The Y46D mutant γC-crystallin also maintains a small radius (1–2 nm) through 46 °C but shows a dramatic increase in particle size to 100–200 nm at 49.5 °C and 200–10,000 nm at 53 and 56.5 °C (Figure 5C). In contrast, a 1:1 molar ratio mixture of Y46D mutant γC-crystallin and αA-crystallin shows a bimodal distribution at 1–2 and 2–20 nm at 32 and 35.5 °C, shifting to a single peak at 2–20 nm at 39–53 °C, and then again to a different bimodal distribution at 2–20 and 100–500 nm at 56.5 °C (Figure 5D), confirming the ability

of αA-crystallin to bind mutant Y46Dcrystallin as it begins to denature at 39 °C and prevent it from forming large aggregates. The increase in aggregate size at 56.5 °C suggests that the αA-crystallin binding capacity is becoming exhausted or overwhelmed.

Association of αA-crystallin with wild-type and mutant γC-crystallin in their native (Figure 6A) and stressed states (Figure 6B) was also checked by analytical size exclusion chromatography. At 25 °C, αA-crystallin alone eluted as a single peak at 9–13 mL (500 kDa) (data not shown), wild-type and Y46D mutant γC-crystallin alone eluted at 15–18 mL (20 kDa) (data not shown), and mixtures of α- and γ-crystallins eluted as two peaks at these locations (Figure 6A). No additional peaks corresponding to higher aggregates were observed at 25 °C, although there was a slight shoulder in the α-crystallin peak. When the proteins were stressed at 45 and 50 °C and loaded to size exclusion chromatography column, the height of the mutant γC-crystallin peak dropped from 180 to 100 mAU, whereas the wild-type γC-crystallin peak continues to show a height of approximately 150 mAU at 45–55 °C, consistent with some Y46D mutant protein and to a lesser degree the wild-type γC-crystallin being lost as an aggregate after heating for 1 h at 55 °C, which is precipitated by centrifugation prior to loading on the column. ESI LC/MS was used to identify the proteins in each peak (Tables S1–S7). At all temperatures for the αA-crystallin + wild-type γC-crystallin samples, the peak at the elution volume 9–13 mL had a mass similar to that of pure αA-crystallin (20729.7 ± 1 Da) and no wild-type γC-crystallin was detected in that range. Similarly, the peak at 15–18 mL displayed only wild-type γC-crystallin (mass 20745.15 ± 0.5 Da). In contrast, although the αA-crystallin + Y46D mutant γC-crystallin sample peak at 9–13 mL (mass 20697.15 ± 0.51 Da) showed only αA-crystallin at 25 and 45 °C, by 50 °C, it also showed compounds consistent with both αA-crystallin and the Y46D mutant γC-crystallin at the leading edge (Table S1). This is consistent with binding of partially denatured Y46D mutant γC-crystallin by αA-crystallin under thermal stress.

DISCUSSION

We have characterized effects of the cataract-associated Y46D mutation on γC-crystallin structure and stability. While this amino acid substitution has only a small effect on the protein fold under benign conditions, it does decrease the stability of the protein significantly, especially that of the amino domain, under thermal or chemical stress. As the accessible surfaces of the Y46 D46 residues are calculated to be 229 and 151 Å^2, respectively,[28] size or crowding is unlikely to be major factors in the loss of stability, although partial unfolding or misfolding of the protein could change the total solvent-accessible surface area much more than the substitution itself. The four aromatic amino acid pairs Y7-F12, Y46-Y51, Y134-Y139, and Y17-Y29 in human γC-crystallin play an important role in providing stable and compact folding for the protein. Of these, three reside in a Greek key motif as Greek key pairs. The Y46D mutation affects the second Greek key pair (Y46-Y51) interaction, has been reported to cause autosomal dominant congenital nuclear cataracts,[15] and thus should provide a good model to understand the molecular mechanisms leading to denaturation of γC-crystallin and thence to lens opacification.

Y46D is the first missense mutation reported in human γC-crystallin in which the mutation affects the second Greek key pair aromatic interaction, resulting in destabilization of the

molecule and changing the overall net charge or pI (isoelectric point) of the protein. Replacing the aromatic amino acid tyrosine with the charged amino acid aspartate is predicted to change the isoelectric point of the protein from 6.88 to 6.43 according to analysis using ExPASyProtParam.[29] The Coulombic interactions of the local amino acids are altered as a result of this displacement and are predicted to affect the π interactions of the second Greek key pair interaction, thereby destabilizing the respective motif, domain, and thence the entire protein. While under benign conditions, the gross secondary structure of γC-crystallin is not altered significantly by the Y46D substitution, alteration of the tryptophan microenvironment is shown by changes in the near-UV CD spectra, which reflect tryptophan and tyrosine environments in the protein and the 1.2-fold increase in tryptophan emission fluorescence.

Similarly, increased fluorescence of the Y46D mutant crystallin in the presence of bis-ANS and Nile Red dyes indicated that the Y46D mutant γC-crystallin has increased surface hydrophobicity relative to the wild-type protein, suggesting that loss of the Y46-Y51 pair results in movement of one or more aromatic amino acids from the hydrophobic protein core so that it becomes exposed to the surface of the molecule. The differences between the wt and Y46D mutant γC-crystallin as shown by bis-ANS and Nile Red are consistent with (although greater in magnitude) results seen in studies of the P23T mutant γD-crystallin by Pande et al.[30] This might be related to possible electrostatic interactions of Bis-ANS with the protein surface, although Bis-ANS binding has been shown to be dominated by hydrophobic interactions.[31]

While not causing a major perturbation of the protein fold in benign conditions, the Y46D mutation decreases the overall stability of the molecule as shown by its behavior when it is subjected to thermal or chemical stress. These results are similar overall to those of Fu et al.,[16,17] who showed that the Y46D mutation decreases the thermal stability of γC-crystallin and that this could be rescued by high concentrations of αA-crystallin. They also showed that the Y46D mutation altered hydrogen bonding in the second Greek key motif and exposed more hydrophobic residues to the surface, resulting in decreased resistance to chemical denaturants, UV light, pH extremes, and oxidative stress, similar to but less severe than a L45P mutation they studied in parallel. While they did not calculate energy changes resulting from the mutations, their results appear similar to those seen in this work.

The decreased thermal stability of the Y46D mutant γC-crystallin is also reflected by its increased light scattering at 65 °C beginning at about 200 s, while the wild-type protein remained transparent. The increased light scattering by the Y46D mutant protein is largely prevented by addition of αA-crystallin, once more indicating binding of the partially denatured Y46D mutant by α-crystallin, and consistent with both the DLS and SEC analyses. However, although Fu et al. showed that the Y46D mutant γC-crystallin shows increased susceptibility to oxidative damage,[16] in this study, reducing agents, including TCEP and DTT, failed to inhibit thermal aggregation of the Y46D mutant γC-crystallin. This contrasts with results seen with other mutant crystallins[32] and suggests that aggregation of the Y46D mutant γC-crystallin might be independent of disulfide bridge formation. It should be noted that while 65° C is near the midpoint of the thermal denaturation curve for

the Y46D mutant γC-crystallin and below that of the wild type, it is possible that a different mechanism of destabilization might occur under more physiological conditions.

Phenyl ring centroids tend to prefer a distance of 4.5–7 Å with dihedral angles approaching 90° (perpendicular interactions) being the most common in many proteins. An aromatic–aromatic pair interaction has an energy of 1–2 kcal mol^{-1}, and buried or partially buried aromatic interactions contribute a free energy of 0.6–1.3 kcal mol^{-1} to protein stability.[14] Aromatic rings in aromatic pairs also can align parallel to each other and this parallel displacement stacking provides 0.5–0.75 kcal mol^{-1} stability to the protein. If both the interacting partners are phenylalanine, the interaction provides a stability of 1 kcal mol^{-1} to the protein.[13] A study on thermophilic proteins revealed that additional aromatic clusters with perpendicular packing symmetry are present on the surface close to the active sites and provide thermostability compared to mesophilic proteins, in which active sites tend to have leucine, serine, or isoleucine instead of aromatic residues in these interactions. This further emphasizes the importance of aromatic pair interactions and their role in highly stable thermophilic proteins.[33] All these studies support the concept that aromatic interactions provide stability to molecules, and loss of the π interactions around the second Greek key pair interaction in the Y46D substitution would be expected to destabilize the molecule and particularly to decrease its resistance to thermal or chemical stress.

Aromatic pairs are known to play an important role in human γD crystallin stability and of these, the Greek key pairs contribute more than those not in Greek keys to the molecule's stability.[12] The same aromatic amino acids contribute to the second Greek key pair (Y46-Y51) in human γD- and γC-crystallin. When alanine is substituted for Y46 in human γD-crystallin, the resultant protein shows a two-state transition under thermal unfolding, with an 8.7 °C decrease in its T_m.[12] Of all the substitutions removing aromatic pairs in the study by Kong and King,[12] the average decrease in T_m is 5.6 °C, and the greatest decrease is 9.6 °C for the Y138A change in the C domain. In the present study, the Y46D γC-crystallin showed a much more severe effect under thermal stress, resulting in a three-state unfolding curve and decreases of 23 and 9.9 °C for first and second transitions, respectively, compared to wild-type γC-crystallin. The greater destabilization seen in this case could relate to the substitution of the charged amino acidic aspartate in γC-crystallin instead of the neutral aliphatic amino acid alanine in γD-crystallin and also relate to differences in the two crystallins themselves. The alanine substitution at Y46 in γD-crystallin resulted in a three-state transition in GuHCl unfolding with concentration midpoints of 1.2 and 2.99 M GuHCl for the first and second transitions, respectively, versus 2.99 for the WT.[12] In this study, the Y46D γC-crystallin shows a similar three-state transition with concentration midpoints around 0.9 and 2.1 M for the first and second transition, respectively. The $\Delta\Delta G$ values for the Y46A substitution in γD-crystallin are −5.5 ± 0.2 and −0.3 ± 0.8 for the first and second transitions, respectively, the second not being significantly different from the wild type. In contrast, the $\Delta\Delta G$ values for the Y46D γC-crystallin are −7.324 ± 0.75 and −3.265 ± 0.78, significantly larger than those for the Y46A change reported for γD-crystallin. Of particular note is the effect on the second transition, which shows essentially no change in Y46A-substituted γD-crystallin but which is significant in Y46D γC-crystallin. In fact, although changes in the C-domain appeared to destabilize both domains, none of the substitutions in the N-domain studied by Kong and King showed a significant change in the

second transition and neither did the G18V mutation studied by Ma et al., which destabilizes the first Greek key motif sterically.[19] Taken as a whole, these data suggest that the Y46D mutation not only destabilizes the second Greek key motif in the N-domain to a greater degree than similar changes of members of aromatic pairs to neutral amino acids but has an additional action in destabilizing the C-domain beyond those of the direct effects on the second Greek key motif of the N-domain.

In contrast, other mutations have shown even greater effects on γC-crystallin than the Y46D change described here. The effect of the Y46D mutation on γC-crystallin structure and stability is not as large as that of the L45P mutation studied by Fu et al.[16,17] and especially the T5P mutation associated with autosomal dominant congenital Coppock-like cataracts. The latter alters the protein conformation even under benign conditions, reduces its solubility and stability,[34] increases its propensity to aggregate with rescue by α-A and α-B-crystallin,[35,36] and exposes hydrophobic patches to its surface so that ATP-dependent proteasome pathway-mediated degradation is induced.[37] The G129C mutation in γC-crystallin, which is associated with autosomal dominant congenital cataracts, shows intermediates at lower median GuHCl concentrations than the wild type and affects cell proliferation and death.[38] In addition, the G129C change causes aggregation at high concentrations and results in vacuoles and incomplete denucleation in transgenic zebrafish lenses.[39] Similarly, the R168W mutation in γC-crystallin, which is associated with autosomal dominant congenital lamellar cataract, resembles the wild type in far and near UV CD spectra but shows a red shift of 14 nm in autofluorescence in benign conditions and enhanced fluorescence in the presence of ANS.[18] While the values are somewhat difficult to compare because of differing presentations, it appears to show three stage denaturation curves with thermal and GuHCl stress, with similar midpoints to the Y46D γC-crystallin mutant in both tests. It also produces light scattering particles at high temperatures beginning at 200 s at 65 °C, similar to the Y46D mutant, which also begins to scatter light after 200 s at 65 °C. Thus, while the comparisons are difficult, the R168W mutant might be somewhat more severe than the Y46D mutant under benign conditions, but with similar thermodynamic stability.[18] Among these examples, there appears to be a rough correlation between the severity of a mutation in terms of its effect on protein stability and the timing and character of the resultant cataracts, with more destabilizing mutations resulting in earlier onset and more severe cataracts. There are, of course, exceptions to this trend, including mutations that affect surface hydrophobicity[30,40] and susceptibility to oxidation and photooxidation[41] with minimal effects on protein stability. In contrast, a F30S mutation in γS-crystallin also results in a triphasic denaturation curve with roughly similar changes in free energy, but while it increases tryptophan fluorescence even under benign conditions, it actually decreases ANS fluorescence, suggesting that fewer hydrophobic residues were exposed to the surface.[42] It should be remembered that there are alternative pathways to βγ-crystallin aggregation besides instability[43,44] as is demonstrated by crystallin mutants mimicking photodamage and age-related cataract models.[45,46]

CONCLUSIONS

In summary, the Y46D γC-crystallin mutant is an example that demonstrates how a point mutation that minimally alters the tertiary structure of βγ-crystallins but increases the

surface hydrophobicity and decreases the stability of the protein toward thermally and chemically induced stress can ultimately lead to light scattering. While the molecule might function and associate normally in the fetal eye, when it is subjected to stress, which in the lens might be just time at body temperature or perhaps oxidative or photo-oxidative even though it might not involve disulfide bond formation,[47] it denatures and forms light scattering aggregates. This process would be predicted to be delayed in the lens not only through the large reservoir of reducing power available in lens cells but also as the forming aggregates would be bound and solubilized, but not renatured, by α-crystallin. As the cellular reservoir of α-crystallin is quickly exhausted with the relatively large decreases in stability seen with this mutation, the bound complexes form high-molecular-weight complexes that are capable of scattering light directly, or eventually of having a toxic effect on the lens cells if they escape or overwhelm α-crystallin binding completely. Overall, the structural and stability changes in γC-crystallin caused by the Y46D mutation explain the probable pathological mechanism behind cataract formation and correlate with the timing and presentation in this family. This provides further insight into the critical role of aromatic pairs in stabilizing Greek key motifs in the $\beta\gamma$-crystallins and other proteins as well as supporting the general correlation between the structural severity of crystallin mutations and the clinical characteristics and timing of the resulting cataract.

Supplementary Material

Refer to Web version on PubMed Central for supplementary material.

Funding

This work was supported by funding from the National Eye Institute, ZIA EY000281-30.

ABBREVIATIONS

LB	Luria Bertani
IPTG	isopropyl-β-D-thiogalactopyranoside
EDTA	ethylenediaminetetraacetic acid
DTT	dithiothreitol
TCEP	tris[2-carboxyethyl]-phosphine
SEC	size exclusion chromatography
SDS-PAGE	sodium dodecyl sulfate polyacrylamide gel electrophoresis
ESI	electrospray ionization
LC/MS	liquid chromatography/mass spectrometry
CD	circular dichroism
DIT	digital integration time

bis-ANS	bis-ANS 4,4′-dianilino-1,1′-binaphthyl-5,5′-disulfonic acid
Nile Red	9-diethylamino-5-benzo[*a*]phenoxazinone
AU	arbitrary units
ME	molar ellipticity
FI	fluorescence intensity
DLS	dynamic light scattering
HMW	high molecular weight
WT	wild type

REFERENCES

(1). Benedek GB Theory of transparency of the eye. Appl. Opt. 1971, 10, 459–473. [PubMed: 20094474]

(2). Mörner CT Untersuchungender protein-substanzen in den lichtbrechenden Medien des Auges. Hoppe-Seyler's Z.Physiol.Chem. 1894, 18, 61–106.

(3). Piatigorsky J Lens crystallins and their gene families. Cell 1984, 38, 620–621. [PubMed: 6548413]

(4). Delaye M; Tardieu A Short-range order of crystallin proteins accounts for eye lens transparency. Nature 1983, 302, 415–417. [PubMed: 6835373]

(5). Hejtmancik JF; Kaiser-Kupfer MI; Piatigorsky J Molecular biology and inherited disorders of the eye lens, In The Metabolic and Molecular Basis of Inherited Disease (Scriver CR; Beaudet AL; Valle D; Sly WS; Childs B; Kinzler KW; Vogelstein B, Eds.), pp. 2001, 6033–6062, McGraw Hill, New York.

(6). Shoshany N; Hejtmancik JF; Shiels A; Datiles M Congenital and Hereditary Cataracts: Epidemiology and Genetics, In Pediatric Cataract Surgery and IOL Implantation (Kraus CL, Ed.), pp. 2020, 3–24, Springer, New York.

(7). Hemmingsen JM; Gernert KM; Richardson JS; Richardson DC The tyrosine corner: a feature of most Greek key beta-barrel proteins. Protein Sci. 1994, 3, 1927–1937. [PubMed: 7703839]

(8). Wistow G; Turnell B; Summers L; Slingsby C; Moss D; Miller L; Lindley P; Blundell T X-ray analysis of the eye lens protein gamma-II crystallin at 1.9 A resolution. J. Mol. Biol. 1983, 170, 175–202. [PubMed: 6631960]

(9). Richardson JS beta-Sheet topology and the relatedness of proteins. Nature 1977, 268, 495–500. [PubMed: 329147]

(10). Hutchinson EG; Thornton JM The Greek key motif: extraction, classification and analysis. Protein Eng. 1993, 6, 233–245. [PubMed: 8506258]

(11). Vendra VPR; Agarwal G; Chandani S; Talla V; Srinivasan N; Balasubramanian D Structural integrity of the Greek key motif in betagamma-crystallins is vital for central eye lens transparency. PLoS One 2013, 8, No. e70336. [PubMed: 23936409]

(12). Kong F; King J Contributions of aromatic pairs to the folding and stability of long-lived human gammaD-crystallin. Protein Sci. 2011, 20, 513–528. [PubMed: 21432932]

(13). McGaughey GB; Gagne M; Rappe AK pi-Stacking interactions, *Alive and well in proteins*. J. Biol. Chem. 1998, 273, 15458–15463. [PubMed: 9624131]

(14). Burley SK; Petsko GA Aromatic-aromatic interaction: a mechanism of protein structure stabilization. Science 1985, 229, 23–28. [PubMed: 3892686]

(15). Zhong Z; Wu Z; Han L; Chen J Novel mutations in CRYGC are associated with congenital cataracts in Chinese families. Sci. Rep. 2017, 7, 189. [PubMed: 28298635]

(16). Fu C; Xu J; Jia Z; Yao K; Chen X Cataract-causing mutations L45P and Y46D promote gammaC-crystallin aggregation by disturbing hydrogen bonds network in the second Greek key motif. Int. J. Biol. Macromol. 2021, 167, 470–478. [PubMed: 33278449]

(17). Fu C; Xu J; Yang X; Chen X; Yao K Cataract-causing mutations L45P and Y46D impair the thermal stability of gammaC-crystallin. Biochem. Biophys. Res. Commun. 2021, 539, 70–76. [PubMed: 33422942]

(18). Talla V; Narayanan C; Srinivasan N; Balasubramanian D Mutation causing self-aggregation in human gammaC-crystallin leading to congenital cataract. Invest. Ophthalmol. Vis. Sci 2006, 47, 5212–5217. [PubMed: 17122105]

(19). Ma Z; Piszczek G; Wingfield PT; Sergeev YV; Hejtmancik JF The G18V CRYGS Mutation Associated with Human Cataracts Increases γS-Crystallin Sensitivity to Thermal and Chemical Stress. Biochemistry 2009, 48, 7334–7341. [PubMed: 19558189]

(20). Vendra VP; Chandani S; Balasubramanian D The mutation V42M distorts the compact packing of the human gamma-S-crystallin molecule, resulting in congenital cataract. PLoS One 2012, 7, No. e51401. [PubMed: 23284690]

(21). Pace CN; Shirley BA; Thomson J Measuring the conformational stability of proteins, In Protein Structure: a Practical Approach (Creighton TE, Ed.), pp. 311–330, IRL Press, Oxford.

(22). Pace CN Determination and analysis of urea and guanidine hydrochloride denaturation curves. Methods Enzymol. 1986, 131, 266–280. [PubMed: 3773761]

(23). Rosen CG; Weber G Dimer formation from 1-amino-8-naphthalenesulfonate catalyzed by bovine serum albumin. A new fluorescent molecule with exceptional binding properties. Biochemistry 1969, 8, 3915–3920. [PubMed: 5388144]

(24). Sutter M; Oliveira S; Sanders NN; Lucas B; van Hoek A; Hink MA; Visser AJ; De SC; Hennink WE; Jiskoot W Sensitive spectroscopic detection of large and denatured protein aggregates in solution by use of the fluorescent dye Nile red. J. Fluoresc. 2007, 17, 181–192. [PubMed: 17294134]

(25). LeVine H 3rd. Quantification of beta-sheet amyloid fibril structures with thioflavin T. Methods Enzymol. 1999, 309, 274–284. [PubMed: 10507030]

(26). Rao PV; Horwitz J; Zigler JS Jr. Alpha-crystallin, a molecular chaperone, forms a stable complex with carbonic anhydrase upon heat denaturation. Biochem. Biophys. Res. Commun. 1993, 190, 786–793. [PubMed: 8094957]

(27). Kosinski-Collins MS; King J In vitro unfolding, refolding, and polymerization of human gammaD crystallin, a protein involved in cataract formation. Protein Sci. 2003, 12, 480–490. [PubMed: 12592018]

(28). Miller S; Janin J; Lesk AM; Chothia C Interior and surface of monomeric proteins. J. Mol. Biol. 1987, 196, 641–656. [PubMed: 3681970]

(29). Duvaud S; Gabella C; Lisacek F; Stockinger H; Ioannidis V; Durinx C Expasy, the Swiss Bioinformatics Resource Portal, as designed by its users. Nucleic Acids Res. 2021, 49, W216–W227. [PubMed: 33849055]

(30). Pande A; Ghosh KS; Banerjee PR; Pande J Increase in surface hydrophobicity of the cataract-associated P23T mutant of human gammaD-crystallin is responsible for its dramatically lower, retrograde solubility. Biochemistry 2010, 49, 6122–6129. [PubMed: 20553008]

(31). Hawe A; Sutter M; Jiskoot W Extrinsic fluorescent dyes as tools for protein characterization. Pharm. Res. 2008, 25, 1487–1499. [PubMed: 18172579]

(32). Serebryany E; Yu S; Trauger SA; Budnik B; Shakhnovich EI Dynamic disulfide exchange in a crystallin protein in the human eye lens promotes cataract-associated aggregation. J Biol Chem 2018, 293, 17997–18009. [PubMed: 30242128]

(33). Kannan N; Vishveshwara S Aromatic clusters: a determinant of thermal stability of thermophilic proteins. Protein Eng. 2000, 13, 753–761. [PubMed: 11161106]

(34). Fu L; Liang JJ-N Conformational change and destabilization of cataract gammaC-crystallin T5P mutant. FEBS Lett. 2002, 513, 213–216. [PubMed: 11904153]

(35). Liu BF; Song S; Hanson M; Liang JJ Protein-protein interactions involving congenital cataract T5P gammaC-crystallin mutant: a confocal fluorescence microscopy study. Exp. Eye Res. 2008, 87, 515–520. [PubMed: 18926820]

(36). Liang JJ Interactions and chaperone function of alphaA-crystallin with T5P gammaC-crystallin mutant. Protein Sci. 2004, 13, 2476–2482. [PubMed: 15322286]

(37). Zhang X; Taylor A; Liu Y; Shang F Glutathiolation Triggers Proteins for Degradation by the Ubiquitin- Proteasome Pathway. Curr. Mol. Med. 2017, 17, 258–269. [PubMed: 29110605]

(38). Xi YB; Chen XJ; Zhao WJ; Yan YB Congenital Cataract-Causing Mutation G129C in gammaC-Crystallin Promotes the Accumulation of Two Distinct Unfolding Intermediates That Form Highly Toxic Aggregates. J. Mol. Biol. 2015, 427, 2765–2781. [PubMed: 26165230]

(39). Li XQ; Cai HC; Zhou SY; Yang JH; Xi YB; Gao XB; Zhao WJ; Li P; Zhao GY; Tong Y; Bao FC; Ma Y; Wang S; Yan YB; Lu CL; Ma X A novel mutation impairing the tertiary structure and stability of gammaC-crystallin (CRYGC) leads to cataract formation in humans and zebrafish lens. Hum Mutat 2012, 33, 391–401. [PubMed: 22052681]

(40). Bharat SV; Shekhtman A; Pande J The cataract-associated V41M mutant of human gammaS-crystallin shows specific structural changes that directly enhance local surface hydrophobicity. Biochem. Biophys. Res. Commun. 2014, 443, 110–114. [PubMed: 24287181]

(41). Wu J; Xu W; Wu W; Xu J; Zheng S; Shentu X; Chen X Cataract-causing mutation R48C increases gammaA-crystallin susceptibility to oxidative stress and ultraviolet radiation. Int. J. Biol. Macromol. 2022, 194, 688–694. [PubMed: 34826455]

(42). Wang KJ; Liao XY; Lin K; Xi YB; Wang S; Wan XH; Yan YB A novel F30S mutation in gammaS-crystallin causes autosomal dominant congenital nuclear cataract by increasing susceptibility to stresses. Int. J. Biol. Macromol. 2021, 172, 475–482. [PubMed: 33454329]

(43). Brubaker WD; Freites JA; Golchert KJ; Shapiro RA; Morikis V; Tobias DJ; Martin RW Separating instability from aggregation propensity in gammaS-crystallin variants. Biophys. J. 2011, 100, 498–506. [PubMed: 21244846]

(44). Rocha MA; Sprague-Piercy MA; Kwok AO; Roskamp KW; Martin RW Chemical Properties Determine Solubility and Stability in betagamma-Crystallins of the Eye Lens. ChemBioChem 2021, 22, 1329–1346. [PubMed: 33569867]

(45). Ji F; Jung J; Koharudin LM; Gronenborn AM The human W42R gammaD-crystallin mutant structure provides a link between congenital and age-related cataracts. J Biol Chem 2013, 288, 99–109. [PubMed: 23124202]

(46). Serebryany E; Takata T; Erickson E; Schafheimer N; Wang Y; King JA Aggregation of Trp > Glu point mutants of human gamma-D crystallin provides a model for hereditary or UV-induced cataract. Protein Sci. 2016, 25, 1115–1128. [PubMed: 26991007]

(47). Spector A Oxidative stress-induced cataract: mechanism of action. FASEB J. 1995, 9, 1173–1182. [PubMed: 7672510]

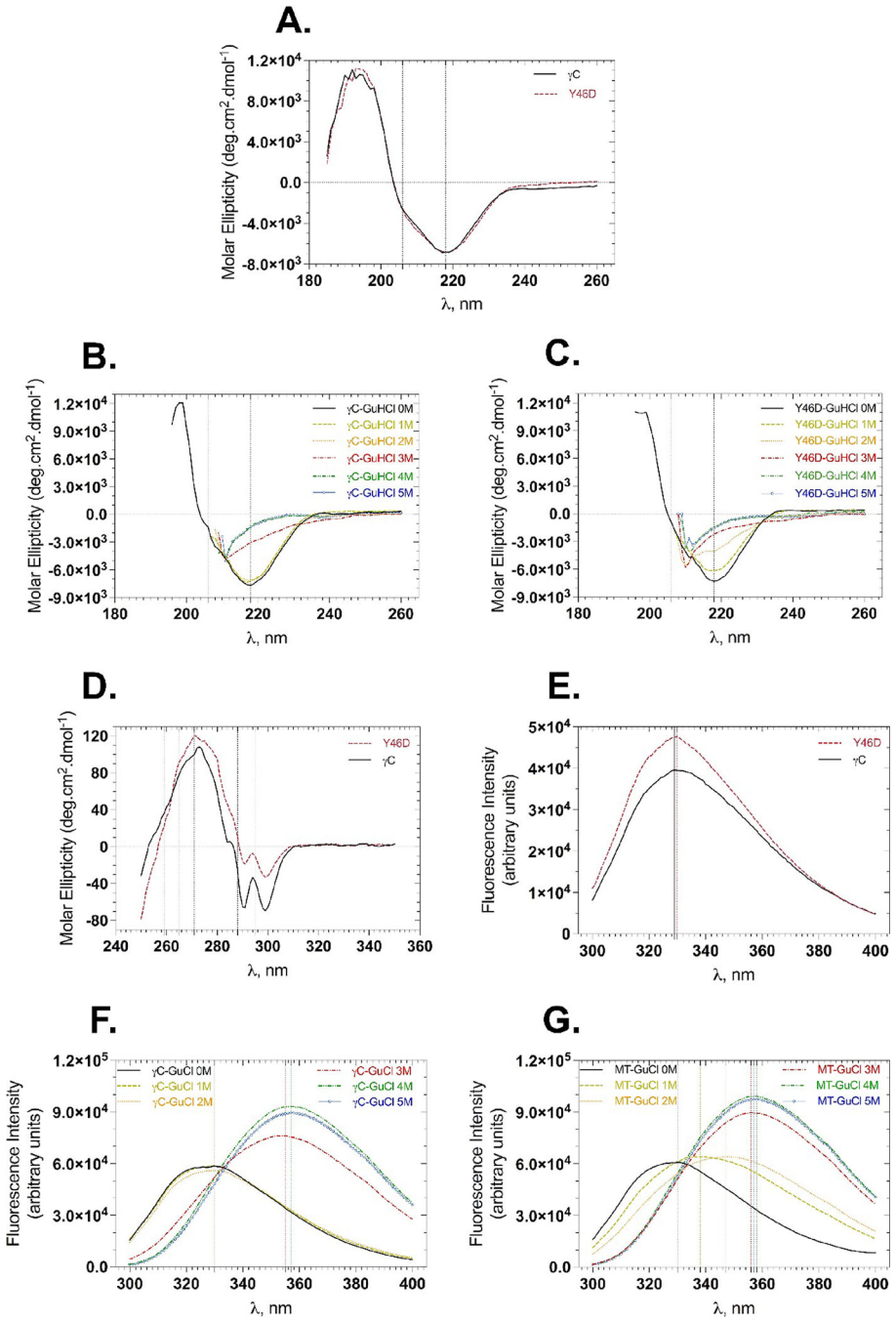

Figure 1.

Secondary and tertiary structural features of wild-type and mutant human γC- crystallin. (A) Far-UV CD spectra of WT (black) and Y46D mutant (maroon) γC-crystallin. Averages of five runs for each protein are presented. Dotted vertical lines at 218 and 206 nm represent the characteristic wavelengths of β-sheet and α-helix, respectively. (B, C) Effect of increasing levels of GuHCl on the molar ellipticity of WT (B) and Y46D (C) γC-crystallin. (D) Near-UV CD spectra of WT (black) and Y46D mutant (maroon) γC-crystallin. Averages of five runs for each protein are presented. Dotted vertical lines

represent tryptophan (295 nm), tyrosine (288 nm), and phenyl alanine (271, 265, 259 nm) environments in the proteins. (E) Fluorescence spectra of WT (black) and Y46D (maroon) γC-crystallin. Dotted vertical lines represent emission maxima of the proteins. (F, G) Effect of increasing levels of GuHCl on the fluorescence spectra of WT (F) and Y46D mutant (G) γC-crystallin.

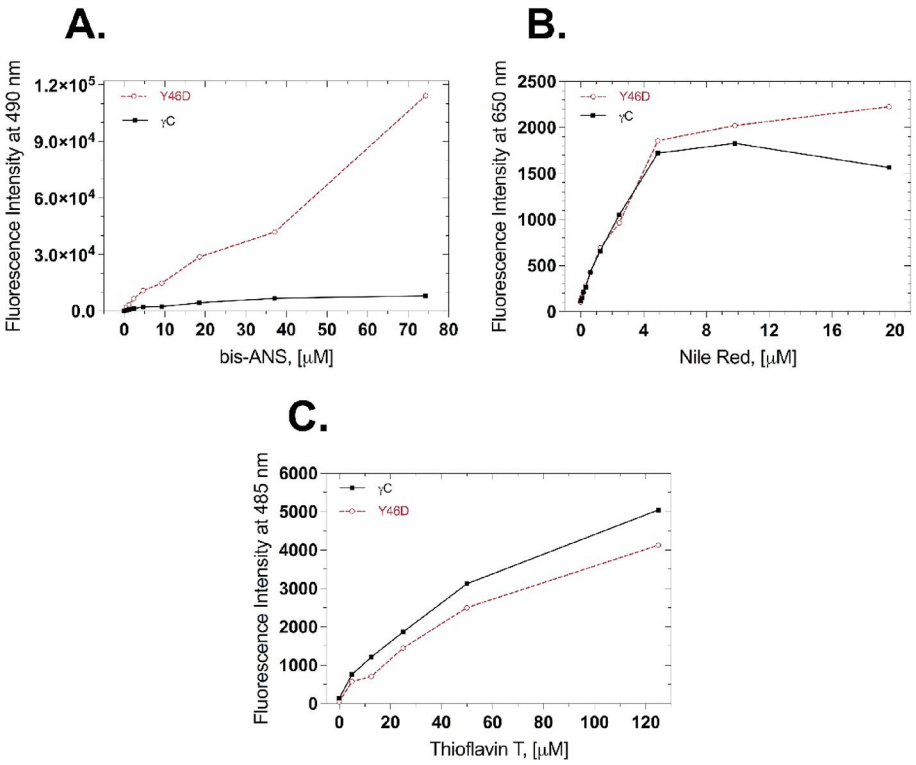

Figure 2.

Surface hydrophobicity and β-structure of wild-type (black) and mutant (maroon) human γC-crystallin Y46D. (A) bis-ANS emission; (B) Nile Red emission; (C) thioflavin fluorescence.

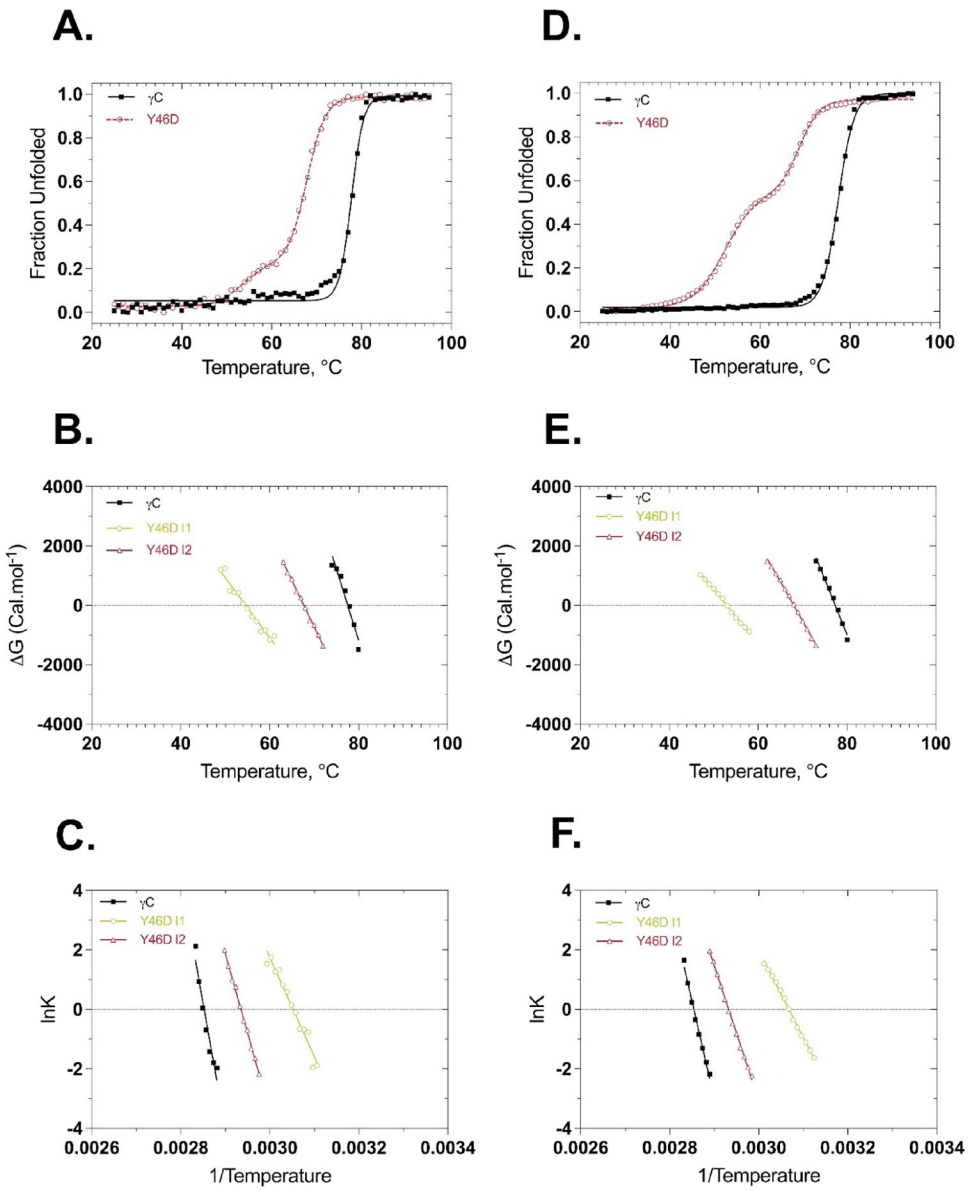

Figure 3.

Thermal denaturation profiles of wild-type (black) and Y46D mutant (maroon) human γC- crystallin by circular dichroism and tryptophan emission fluorescent spectroscopy. (A) Unfolding curves by CD. (B) Δ*G* values calculated from the plot above (panel (A)) as a function of temperature. (C) Van't Hoff plots of the data shown in panel (A). (D) Thermal unfolding curves monitored by tryptophan emission. (E) Δ*G* values calculated from the plots above (panel (D)) as a function of temperature. (F) Van't Hoff plots of the data shown in panel (D).

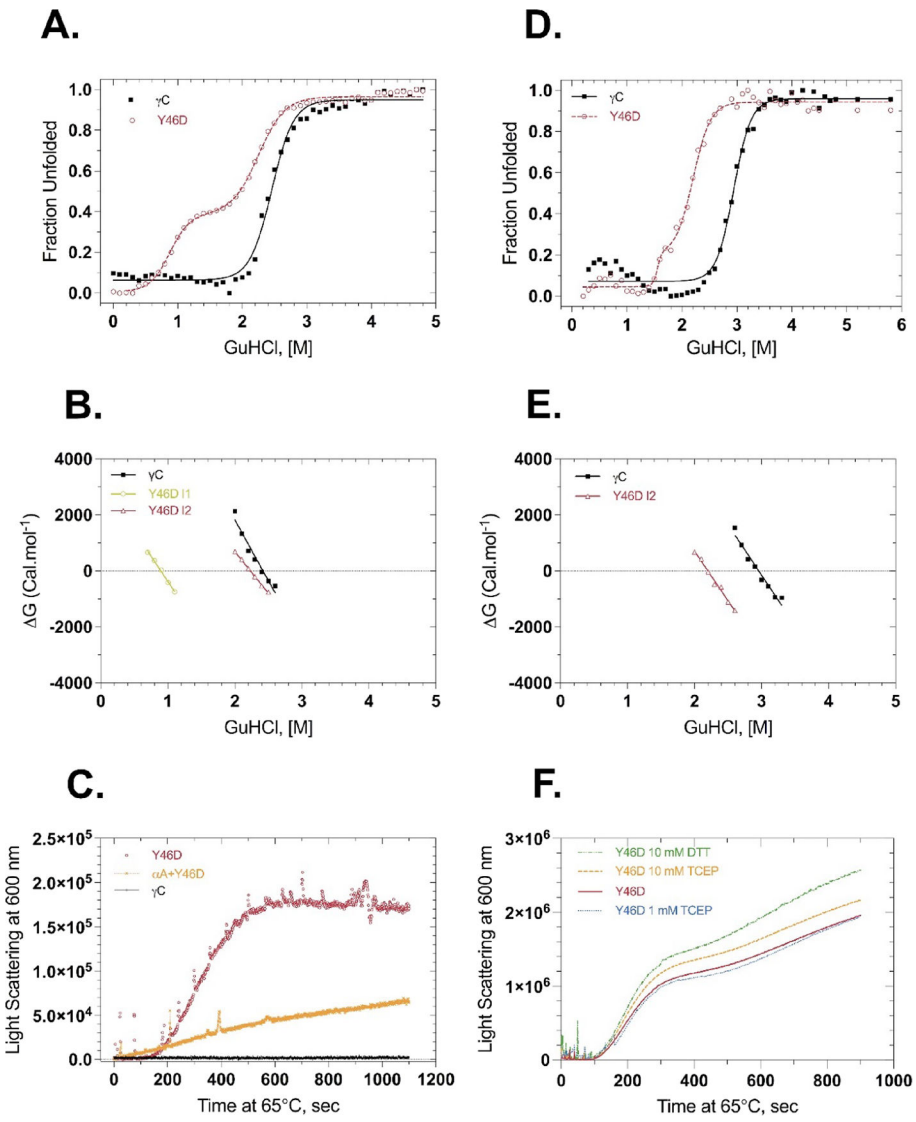

Figure 4.

GuHCl equilibrium unfolding and refolding of wild-type (black) and mutant (maroon) human γC-crystallin Y46D probed by tryptophan fluorescence emission and effects of αA-crystallin and reducing agents on light scattering. (A) GuHCl unfolding curves. (B) Δ*G* values calculated from the above GuHCl denaturation curves shown in (A) as a function of GuHCl concentration. (C) Effect of αA-crystallin on light scattering by Y46D mutant γC-crystallin. (D) GuHCl refolding curves: (E) ΔG values calculated from the refolding curves shown in (D) as a function of GuHCl concentration. (F) Effect of reducing agents on light scattering of the Y46D mutant γC-crystallin over time at 65 °C. Solid lines in (A) and (D) represent two or three-state fits and error bars for the equilibrium unfolding and refolding.

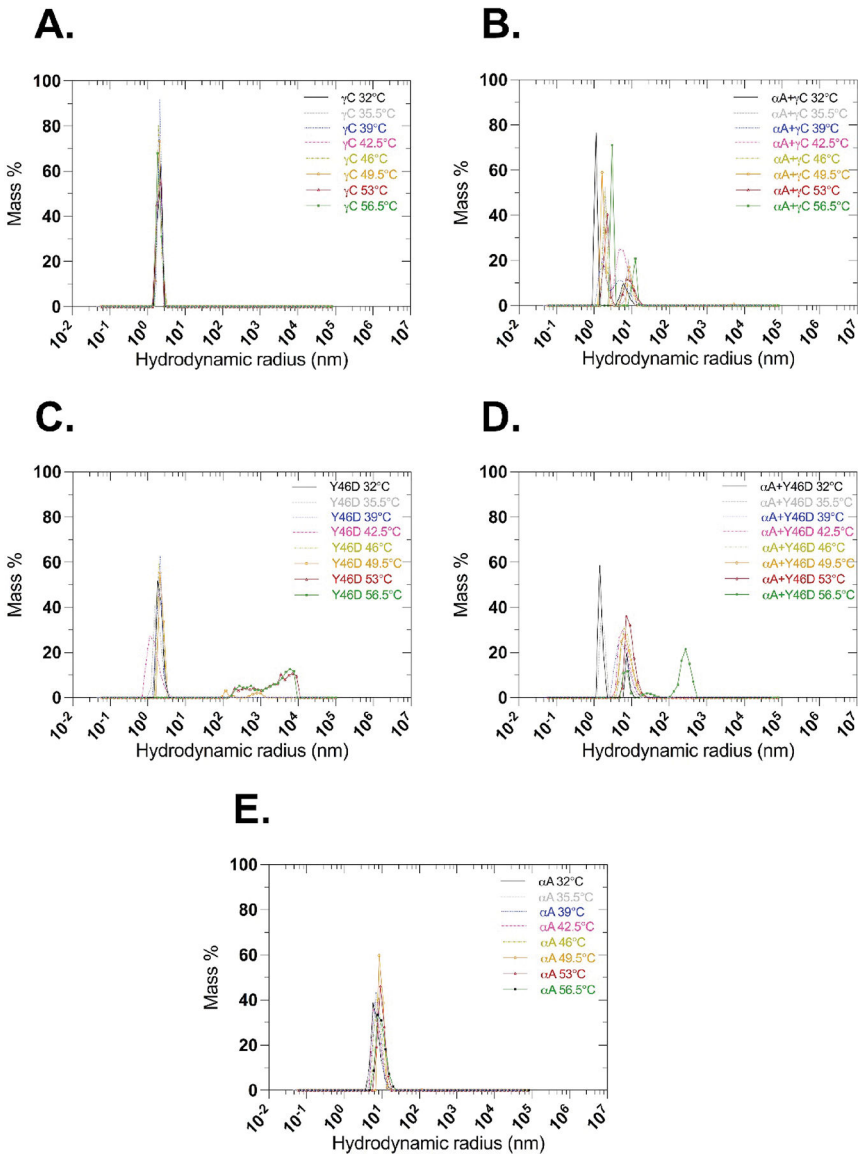

Figure 5.

Particle size at different temperatures measured by dynamic light scattering. (A) γC-crystallin, (B) γC-crystallin + αA-crystallin at a 1:1 molar ratio, (C) Y46D γC-crystallin, (D) Y46D γC-crystallin + αA-crystallin at a 1:1 molar ratio, and (E) αA-crystallin.

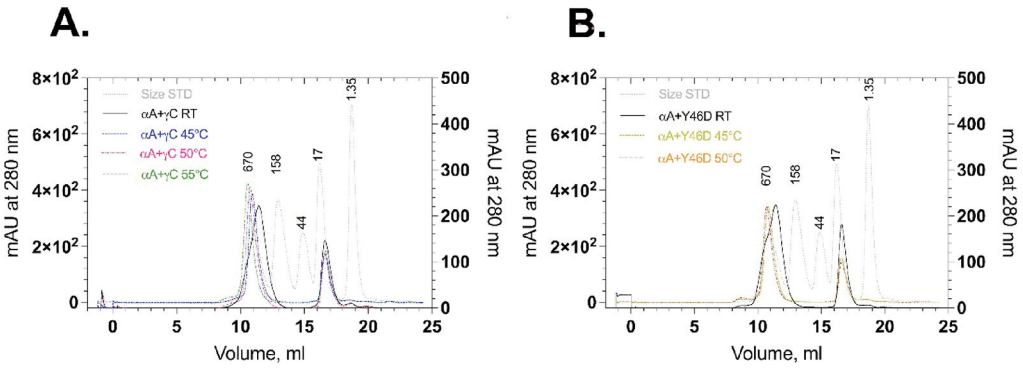

Figure 6.

Size exclusion chromatography profiles of wild-type γC-crystallin and Y46D γC-crystallin mutant γC-crystallin. Superimposed tracings of the size standard alone are shown in a purple dotted line. (A) Association of αA-crystallin with wild type γC-crystallin incubated at room temperature (black), 45 °C (blue), 50 °C (red), and 55 °C (green). (B) Association of αA-crystallin with Y46D mutant human γC-crystallin incubated at room temperature (black), 45 °C (green), and 50 °C (orange). The left and right axes represent mAU for the crystallins and size standards, respectively.

Table 1.

Thermodynamic Values Calculated from the Thermal Unfolding Curves Shown in Figure 3

protein	T_m [a]	ΔT_m [b]	ΔS_m [c]	ΔH_m [d]	$\Delta(\Delta G)$ [e]
WT (CD curve) N↔U	77.6		0.478 ± 0.051	167.6	
MUT (CD curve) N↔I	54.6	−23	0.202 ± 0.013	66.2	−11
MUT (CD curve) I↔U	67.7	−9.9	0.311 ± 0.066	106.1	−4.7
WT (FI ratio curve) N↔U	77.4		0.372 ± 0.017	130.3	
MUT (FI ratio curve) N↔I	52.9	−24.4	0.181 ± 0.032	58.9	−9.1
MUT (FI ratio curve) I↔U	68	−9.3	0.264 ± 0.043	90.1	−3.5

[a] Midpoint of the thermal unfolding curve in °C.

[b] Difference of T_m compared to the wild type in °C.

[c] Slope of (ΔG) versus T in (kcal mol^{-1} deg^{-1}).

[d] ΔH_m = [T_m (K) (ΔS_m)] in (kcal mol^{-1}).

[e] $\Delta(\Delta G)$ = [T_m ΔS_m where ΔS_m is the value for the wild-type protein in kcal mol^{-1}.

Table 2.

Thermodynamic Values Calculated from the GuHCl Unfolding and Refolding Curves Shown in Figure 4

protein	c_m [a]	$\Delta G°$ (kcal mol^{-1})[b]	m (kcal mol^{-1} M^{-})[c]
WT (UF)	2.4	10.503 ± 0.9692	4.339 ± 0.4198
MUT N↔I (UF)	0.9	3.218 ± 1.288	3.591 ± .1413
MUT I↔U (UF)	2.1	6.171 ± 0.1921	2.980 ± 0.0934
WT (RF)	3	10.647 ± 0.831	3.597 ± 0.281
MUT (RF)	2.2	7.767 ± 0.390	3.532 ± 0.169

[a] Midpoint of GuHCl unfolding curve in M.

[b] Free energy of unfolding in the absence of GuHCl in (kcal mol^{-1}).

[c] Slope of GuHCl versus FI ratio in (kcal mol^{-1} M^{-1}).